



A Journal of the Gesellschaft Deutscher Chemiker

Angewandte Chemie

GDCh

International Edition

www.angewandte.org

Accepted Article

Title: Isostructural 3D Covalent Organic Frameworks

Authors: Cheng Wang, Chao Gao, Jian Li, Sheng Yin, Guiqing Lin, Tianqiong Ma, Yi Meng, and Junliang Sun

This manuscript has been accepted after peer review and appears as an Accepted Article online prior to editing, proofing, and formal publication of the final Version of Record (VoR). This work is currently citable by using the Digital Object Identifier (DOI) given below. The VoR will be published online in Early View as soon as possible and may be different to this Accepted Article as a result of editing. Readers should obtain the VoR from the journal website shown below when it is published to ensure accuracy of information. The authors are responsible for the content of this Accepted Article.

To be cited as: *Angew. Chem. Int. Ed.* 10.1002/anie.201905591
Angew. Chem. 10.1002/ange.201905591

Link to VoR: <http://dx.doi.org/10.1002/anie.201905591>
<http://dx.doi.org/10.1002/ange.201905591>

Isostructural 3D Covalent Organic Frameworks

Chao Gao,^{[a]†} Jian Li,^{[b],[c]†} Sheng Yin,^[a] Guiqing Lin,^[a] Tianqiong Ma,^[b] Yi Meng,^[a] Junliang Sun^{*[b],[c]} and Cheng Wang^{*[a]}

Abstract: The construction of high quality three-dimensional covalent organic frameworks (3D COFs) has been considered as a big challenge, especially in how to modify the pore environment and determine the crystal structure to the atomic level. Herein, we reported the designed synthesis of three isostructural 3D COFs functionalized with organic groups –H, –Me and –F, which have similar crystallinity and topology. The crystal structures of these three isostructural 3D COFs were successfully determined by using continuous rotation electron diffraction (cRED) technique, and all the three 3D COFs are identified to adopt a five-fold interpenetrated **pts** topology. More importantly, the resolution of these cRED datasets was measured up to 0.9-1.0 angstrom, leading to the location of all non-hydrogen atomic positions in COF framework directly by 3D ED techniques for the first time. In addition, the precise control of pore environments with different functional groups introduced different selectivity of CO₂ over N₂. In particular, 3D COF with C-F bonds on the pore surface shows the highest selectivity value. This study proved that polycrystalline COFs can also be studied to the atomic level as other materials for the first time and will definitely inspire us to design and synthesize 3D COFs with tailored pore environment for interesting application in future.

Introduction

Covalent organic frameworks (COFs), in which molecular building blocks are precisely organized into two-dimensional (2D) layered structures or three-dimensional (3D) networks, have emerged as a novel class of crystalline organic polymers with inherent porosity and structural periodicity.¹ Owing to their tunable structures and high porosity, COFs have gained great interest and shown promising applications in molecule storage and separation,² heterogeneous catalysis,³ sensing,⁴ energy storage,⁵ optoelectronics,⁶ etc. We should point out that, since Yaghi and co-worker reported the first example in 2005,⁷ most efforts in this attractive area have been devoted on 2D COFs.⁸ By contrast, 3D COFs are much less reported,^{9–13} mainly due to their synthetic challenges and complicated structure determination. However, as 3D COFs can possess numerous open sites and allow hierarchical arrangement of nanopores,

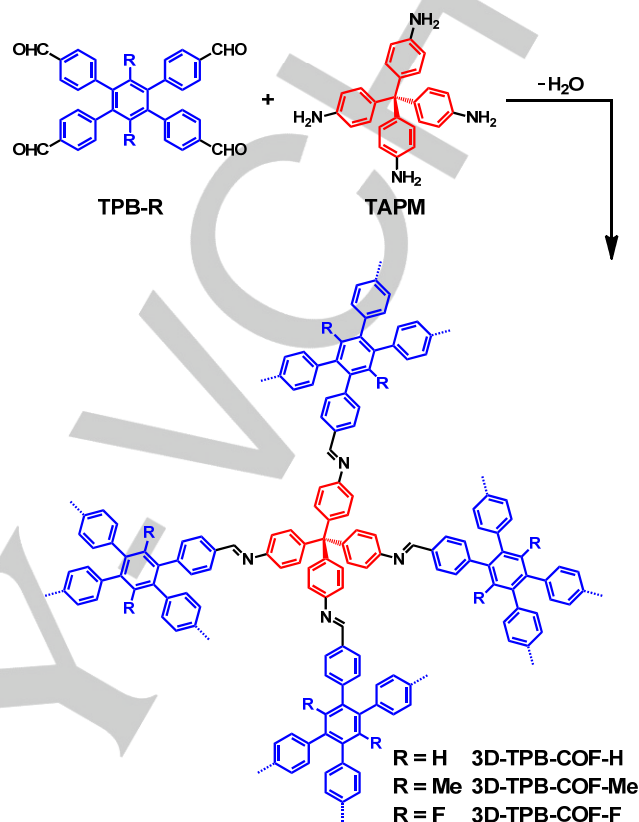


Figure 1. Schematic representation of the synthesis of 3D-TPB-COF-H, 3D-TPB-COF-Me and 3D-TPB-COF-F.

these 3D architectures have found interesting applications and received considerable attention recently. For example, Yan and co-workers claimed that 3D based-functionalized COFs can be used as shape-selective catalysts.^{9e} Yaghi and co-workers reported a 3D COF that should be the first material to be woven at molecular level.^{9f} We also demonstrated that the incorporation of fluorophores into 3D COFs can endow the resulting materials with fluorescence, whereas the 2D COFs analogues are non-fluorescent.^{10a} Considering their unique properties, the construction and functionalization of 3D COFs are highly desirable.

As a kind of highly ordered porous materials, the chemical environment within the pores of 3D COFs is crucial for their applications. Therefore, it is highly demanded to tailor their internal surfaces with desired functionalities. In principle, there are two ways to achieve this goal, either by direct synthesis of 3D COFs from pre-designed precursors with specific functional groups or through post-synthetic modification¹¹ of a pre-made functional 3D COF. For the latter route, functional groups can be anchored onto the surfaces of 3D COF after it has been synthesized and very few examples have been successfully announced until now. Unfortunately, these reported systems usually suffer problems, such as decreasing of crystallinity^{11b} or low conversion yield^{11c}. On the contrary, the former way

[a] C. Gao, S. Yin, G. Lin, Y. Meng, Prof. Dr. C. Wang
Sauvage Center for Molecular Sciences and Key Laboratory of
Biomedical Polymers (Ministry of Education)
College of Chemistry and Molecular Sciences
Wuhan University, Wuhan, China
E-mail: chengwang@whu.edu.cn

[b] Dr. J. Li, Dr. T. Ma, Prof. Dr. J. Sun
College of Chemistry and Molecular Engineering
Beijing National Laboratory for Molecular Sciences
Peking University, Beijing 100871, China
E-mail: junliang.sun@pku.edu.cn

[c] Dr. J. Li, Prof. Dr. J. Sun
Department of Materials and Environmental Chemistry
Stockholm University, Stockholm 10691, Sweden

[†] These authors contributed equally to this work.

Supporting information for this article is given via a link at the end of the document.

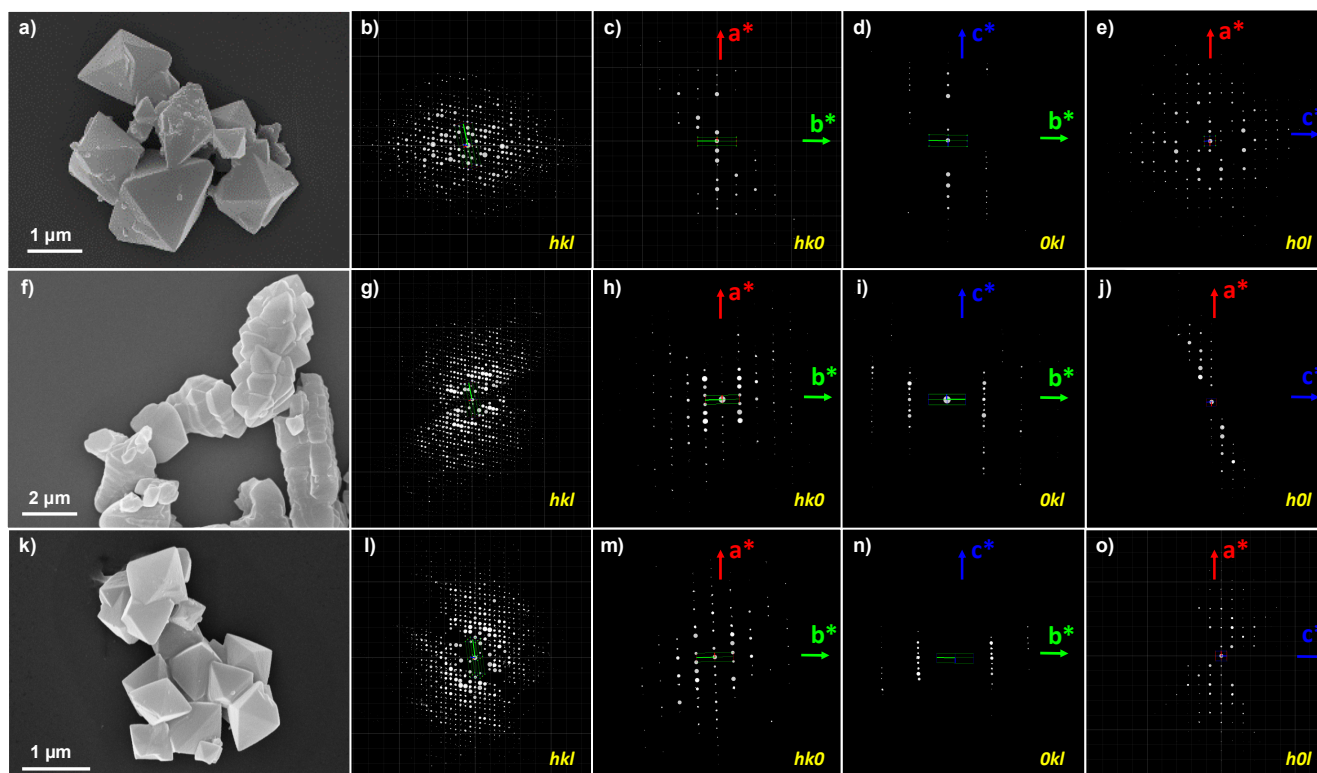


Figure 2. SEM images of 3D-TPB-COF-H (a), 3D-TPB-COF-Me (f) and 3D-TPB-COF-F (k). 3D reciprocal lattice of 3D-TPB-COF-H (b), 3D-TPB-COF-Me (g) and 3D-TPB-COF-F (l). (h0l) (c), (0kl) (d), and (hk0) (e) slices cut from the reconstructed reciprocal lattice of 3D-TPB-COF-H. (h0l) (h), (0kl) (i), and (hk0) (j) slices cut from reconstructed reciprocal lattice of 3D-TPB-COF-Me. (h0l) (m), (0kl) (n), and (hk0) (o) slices cut from the reconstructed reciprocal lattice of 3D-TPB-COF-F.

can overcome these drawbacks, if the functional groups are compatible with the synthetic conditions required to construct the targeted 3D COFs. However, due to the limited diversity of building blocks, the rational design and synthesis of isostructural 3D COFs with different functional groups have been considered as a big challenge. Moreover, once these isostructural 3D COFs are successfully synthesized, another big challenge that has to face is how to resolve their crystal structures at the atomic level to reveal the different functional groups, which cannot be distinguished by using common simulation methods. One possible way is to grow large well-crystalline single crystals for the single crystal X-ray diffraction (SC-XRD), but it took really long time to optimize the synthesis condition^{12a}, the other is to synthesize well crystalline powder samples and hopefully atomic resolution can be reached through powder X-ray diffraction (PXRD) or 3D electron diffraction (ED) techniques.¹⁴ Unfortunately, all reported polycrystalline COFs has relatively low resolution limited to about 1.5-2 angstrom even with the state-of-art 3D ED techniques^{9d,10c,12b}.

Herein, we demonstrate the design and synthesis of three isostructural 3D COFs (Figure 1), in which the pore environment has been finely tuned without changing the topology and interpenetration degree. By selectively choosing the precursors and connection patterns, three isostructural 3D COFs functionalized with organic groups $-H$, $-Me$ and $-F$, have been synthesized. By using continuous rotation electron diffraction (cRED) technique,¹⁵ the resolution of these 3D ED datasets

reached up to 0.9-1.0 angstrom leading to the location of all non-hydrogen atoms directly from a polycrystalline sample for the first time. All three isostructural 3D COFs adopt a five-fold interpenetrated **pts** topology and due to the precise control of pore environments, these 3D COFs exhibit different gas absorption behaviors, e.g., selectivity of CO_2 over N_2 . In particular, 3D COF with C-F bonds on the pore surface shows the highest selectivity value.

Results and Discussion

In order to construct such isostructural 3D COFs, the starting building blocks should have the same skeleton with different functionalities, similar solubility and reactivity. Recently, we demonstrated that it is reasonable to synthesize 3D COFs, starting from tetrahedral and quadrilateral building blocks connected through [4 + 4] imine condensation reactions.¹⁰ Therefore, we decided to choose 1,2,4,5-tetraphenylbenzene (TPB) as the quadrilateral core, as it is possible to modify the 3,6-position of the central benzene ring with different functional groups.^{16a} Accordingly, we designed and synthesized three tetraaldehyde functional TPB derivatives (Figure S1-S3) with organic groups $-H$, $-Me$ or $-F$. As shown in Figure 1, after condensation of tetra(p-aminophenyl)methane (TAPM)^{16b} and the designed TPB analogues, three isorecticular 3D COFs, denoted as 3D-TPB-COF-H, 3D-TPB-COF-Me and 3D-TPB-

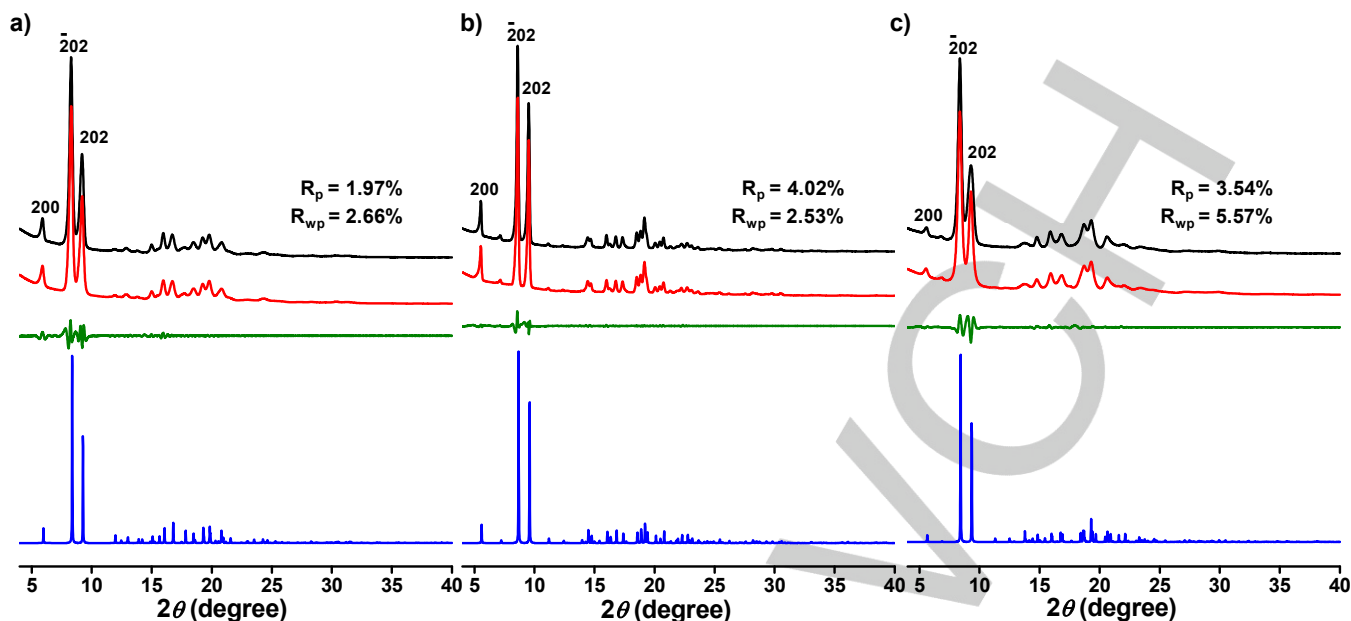


Figure 3. PXRD patterns and Rietveld refinement of (a) 3D-TPB-COF-H, (b) 3D-TPB-COF-Me and (c) 3D-TPB-COF-F. The experimental XRD patterns are shown in black, the Rietveld refinement patterns in red, and their difference in green, the patterns calculated from the five-fold interpenetrated pts net in blue.

COF-F, were successfully isolated as white powders. It should be noted that, in order to obtain high crystalline materials for 3D ED techniques, the synthesis condition, including the reaction solvents, temperature and concentration of acid, must be adaptable to the change of functional TPB precursors, accordingly.

The atomic-level formation of these three isorecticular 3D COFs was confirmed by Fourier transform infrared (FT-IR) spectroscopy and solid-state nuclear magnetic resonance (ssNMR) spectroscopy. According to the FT-IR spectra, all the 3D-TPB-COFs exhibited a stretching vibration band at $\sim 1626\text{ cm}^{-1}$ (Figure S4), indicating the formation of imine bonds. From the ssNMR spectra, new signals appeared at $\sim 160\text{ ppm}$ for all the 3D-TPB-COFs, confirming again the successful formation of imine bonds. In addition, signals at $\sim 64\text{ ppm}$ was found, which should be assigned to the quaternary carbon atom from the TAPM precursor (Figure S5-S7). According to the thermogravimetric analysis (Figure S8), all the 3D-TPB-COFs showed high thermal stability up to about $530\text{ }^{\circ}\text{C}$ under nitrogen. Moreover, scanning electron microscopy (SEM) experiments showed that these 3D-TPB-COFs have a homogeneous morphology with a maximal crystal dimension of $\sim 1\text{ }\mu\text{m}$ (Figure 2a, 2f, 2k, Figure S9).

The crystalline nature of these isorecticular 3D-TPB-COFs was confirmed by PXRD analysis. As shown in Figure 3, all the 3D-TPB-COFs showed amounts of intense diffraction peaks, indicating the long-range ordering. As the crystal sizes for all 3D-TPB-COFs are still too small to collect single crystal X-ray diffraction data (Figure 2a, 2f, 2k), we then decided to use 3D ED technique, which has recently been applied as a powerful tool for the structure determination of 3D COFs^{9d,10c,12b}. cRED data of all the 3D-TPB-COFs single crystals were collected on JEM2100 TEM at 99K by continuously rotating the goniometer.

The cRED data was then processed and intensities were extracted using XDS-data procession software,^{17a} resulting in 3D ED data of up to 1.0, 0.9 and 1.0 angstrom resolution for 3D-TPB-COF-H, 3D-TPB-COF-Me and 3D-TPB-COF-F, respectively. As the average bond length of C-H, C=C, C-F and C-C are 0.96, 1.38, 1.37 and 1.53 angstrom, such high-resolution cRED data are good enough to locate the non-hydrogen atoms and distinguish the group of -H and -Me/-F. The 3D reciprocal lattice of 3D-TPB-COFs (Figure 2b, 2g, 2l) was then reconstructed from the ED patterns by using RED-data processing software.^{17b} The unit cell of 3D-TPB-COFs were determined as monoclinic with $a = 30.25\text{ }\text{\AA}$, $b = 7.52\text{ }\text{\AA}$, $c = 27.10\text{ }\text{\AA}$, and $\beta = 91.45^{\circ}$ for 3D-TPB-COF-H, $a = 30.99\text{ }\text{\AA}$, $b = 7.72\text{ }\text{\AA}$, $c = 26.49\text{ }\text{\AA}$, and $\beta = 90.84^{\circ}$ for 3D-TPB-COF-Me, and $a = 30.75\text{ }\text{\AA}$, $b = 7.68\text{ }\text{\AA}$, $c = 26.64\text{ }\text{\AA}$, and $\beta = 91.45^{\circ}$ for 3D-TPB-COF-F. The same reflection conditions ($hk0: h+k=2n$; $h0l: h=2n, l=2n$) were obtained from the 3D ED data of 3D-TPB-COF-H, 3D-TPB-COF-Me, and 3D-TPB-COF-F, suggesting two possible space groups, $C2/c$ (No.15) and Cc (No.9) (Figure 2b-2e, Figure 2g-2j, Figure 2l-2o). Ab initio structure solutions were then performed with each of the 3D ED data, using the software of *SHELXT*.^{17c} All non-hydrogen atoms, including the function group of -Me/-F, could be directly located with the space groups $C2/c$ in initial structural model (Figure S11, S14, S17). The same initial structure models could also be obtained by Superflip.^{17d} To our best knowledge, this is the first time to locate all non-hydrogen atoms in three 3D COFs from the structure solution and distinguish the function group of -Me/-F and H directly by single crystal electron diffraction (SCED). Finally, 3D-TPB-COF-H, 3D-TPB-COF-F, and 3D-TPB-COF-Me have the same topology with five-fold interpenetrated pts net (Figure 4, Figure S13, S16, S19).

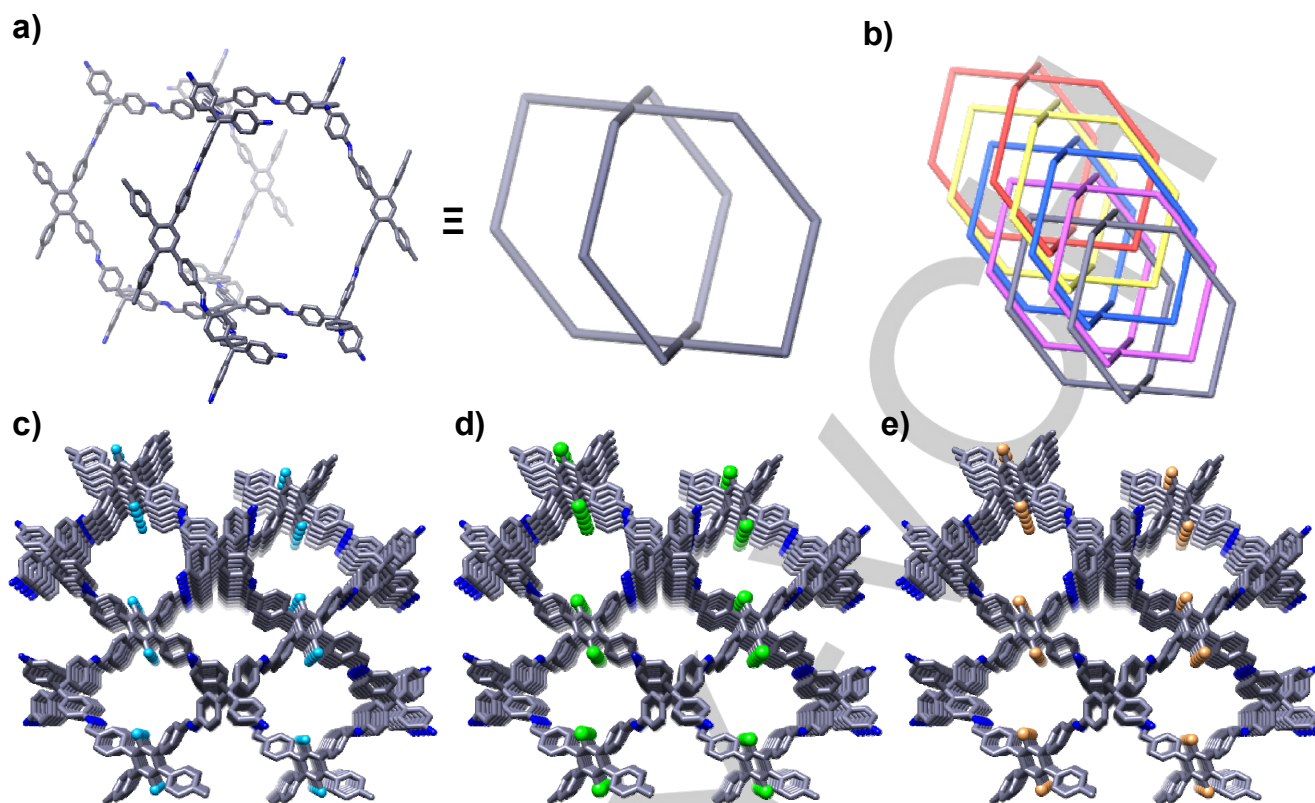


Figure 4. Structural representations of 3D-TPB-COFs. (a) Single pts network of 3D-TPB-COFs; (b) five-fold interpenetrated pts topology; the porous structure of (c) 3D-TPB-COF-H, (d) 3D-TPB-COF-Me and (e) 3D-TPB-COF-F. The carbon is colored in gray and nitrogen is in blue; all the hydrogen atoms are omitted for clarity except the hydrogens in the central benzene rings of 3D-TPB-COF-H. The balls in 3,6-position of the central benzene ring of TPB are the functional groups: H, deep sky blue; Me, green; F, sandy brown.

Structure refinement was subsequently performed against cRED data using *SHELXL* software package.^{17c} All the carbon, nitrogen and fluorine atoms were refined isotropically, with soft restraints for the geometry of the phenyl ring and the C-C and C=N bond lengths. In order to remove the contribution of diffraction from the disordered guest molecules in the pores, the PLATON/SQUEEZE^{17e} procedure was conducted during the refinement. The final R_1 values were converged to 0.3213, 0.2897 and 0.3133 for 3D-TPB-COF-H, 3D-TPB-COF-Me and 3D-TPB-COF-F, respectively (the crystallographic data and structure refinement details performed on cRED data were shown in Table S1, S4 and S7). Due to the presence of dynamical effects and other errors in electron diffraction intensities, the R -Values were relatively high comparing to those in X-ray crystallography. The Rietveld refinement with rigid-body constraints was further performed on the experimental PXRD of these three 3D-TPB-COFs. Although these three 3D-TPB-COF were isostructural with the same topology, the weak peaks of the PXRD were totally different because of the presence of different functional group (Figure 3), i.e. when using the structure model with wrong functional group, the Rietveld refinement will result in higher R -values. Thus, the functional group of –Me/–F and –H could also be easily distinguished by PXRD. The R_{wp} and R_p of final Rietveld refinement were converged to 2.66% and 1.97%

for 3D-TPB-COF-H, 4.02% and 2.53% for 3D-TPB-COF-Me, 5.57% and 3.54% for 3D-TPB-COF-F (the detailed data were shown in Table S2-S3, Table S5-S6 and Table S8-S9).

The permanent porosity of these isostructural 3D-TPB-COFs were investigated by measuring nitrogen (N_2) sorption isotherms at 77 K. As can be seen in Figure S10, all three 3D-TPB-COFs exhibited a type I isotherm with a sharp increase in gas uptake under low relative pressures, indicating their microporous structures. The Brunauer–Emmett–Teller (BET) surface areas were calculated to be $1050 \text{ m}^2 \text{ g}^{-1}$ for 3D-TPB-COF-H, $950 \text{ m}^2 \text{ g}^{-1}$ for 3D-TPB-COF-Me and $850 \text{ m}^2 \text{ g}^{-1}$ for 3D-TPB-COF-F, and the total pore volumes were estimated to be $0.49 \text{ cm}^3 \text{ g}^{-1}$, $0.45 \text{ cm}^3 \text{ g}^{-1}$, and $0.42 \text{ cm}^3 \text{ g}^{-1}$, respectively. Furthermore, the pore-size distributions of these 3D-TPB-COFs were also calculated by using the model of nonlocal density functional theory (NLDFT). Interestingly, 3D-TPB-COF-H showed a major peak centered at 0.56 nm, where 3D-TPB-COF-Me and 3D-TPB-COF-F displayed a major peak at 0.52 nm. This pore size difference can be explained by the volume effect, as –Me and –F groups occupy much more space than H atom.

Given that these isostructural 3D-TPB-COFs possess similar structure, porosity, pore size and thermal stability, we decided to investigate their gas absorption and separation properties to verify the effects of functional groups on pore environment. As a

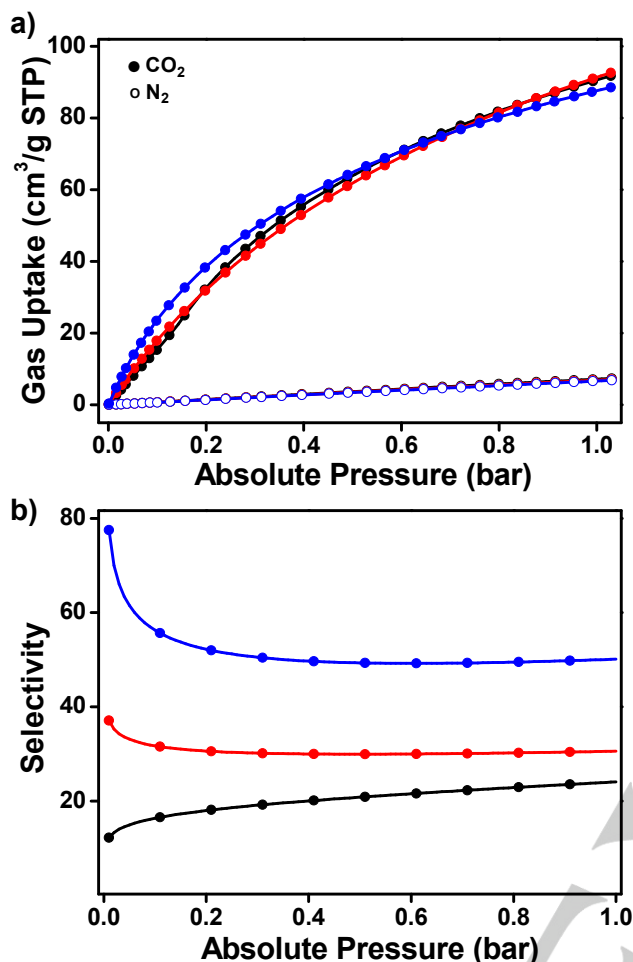


Figure 5. Gas uptake and selectivity of 3D-TPB-COFs. (a) CO₂ and N₂ isotherms at 273 K, full symbols are for CO₂, empty symbols are for N₂; (b) IAST selectivity of CO₂/N₂ at the ratio of 15/85. Note: 3D-TPB-COF-H (black), 3D-TPB-COF-Me (red), 3D-TPB-COF-F (blue).

proof-of-concept study, we chose to investigate the selective sorption of CO₂ over N₂, since CO₂ has larger quadrupole moment than that of N₂. The N₂ uptakes of 3D-TPB-COFs at 273 K are all very low due to the weak interaction between the framework and N₂, as shown in Figure 5a. In contrast, all three 3D-TPB-COFs can adsorb much more amount of CO₂ with almost the same value (~90 cm³ g⁻¹) at 273 K and 1 bar. More importantly, 3D-TPB-COF-F shows much more adsorption at low CO₂ pressure than 3D-TPB-COF-H and 3D-TPB-COF-Me. In order to further understand the CO₂ adsorption properties, we calculated the isosteric heat of adsorption (Q_{st}) from the CO₂ adsorption isotherms at temperatures of 273 K and 298 K by fitting the data to virial equation (Table S10 and Figure S21-S23). At zero coverage, the Q_{st} value of 3D-TPB-COF-H, 3D-TPB-COF-Me and 3D-TPB-COF-F were calculated to be 21.8 kJ mol⁻¹, 24.7 kJ mol⁻¹ and 28.4 kJ mol⁻¹, respectively, which explains the high adsorption of CO₂ for 3D-TPB-COF-F at low pressure.¹⁸ On the basis of the CO₂ and N₂ isotherms measured at 273 K, we then used the ideal adsorbed solution theory (IAST) to calculate the multicomponent adsorption behavior. The

adsorption selectivity for CO₂/N₂ mixtures (15/85) of 3D-TPB-COFs as a function of pressure was presented in Figure 5b. Obviously, 3D-TPB-COF-F showed a selectivity of 50 at 1 bar, which is higher than that of 3D-TPB-COF-Me (31, 1 bar) and 3D-TPB-COF-H (24, 1 bar). Thus, by changing the pore environment of 3D-TPB-COFs, the selective sorption capability can be definitely tuned.

Conclusion

In summary, we have designed and synthesized three isostructural 3D-TPB-COFs, in which the pore environment has been precisely tuned leading to the highest selectivity of CO₂ over N₂ with polar C-F functional groups. With state-of-art cRED techniques, the electron diffraction resolution reached up to 0.9–1.0 angstrom, which gives the possibility to locate all non-hydrogen atoms directly from a polycrystalline sample for the first time. Three 3D-TPB-COFs were proved to adopt the same five-fold interpenetrated pts topology with clearly visible different functional groups. This result can not only help us for better understanding and future designing of the pore environment of 3D COFs for targeted applications, but also open the possibility to study the polycrystalline COF samples directly at atomic level while avoiding the growth of large COF single crystals.

Experimental Section

Synthesis of 3D-TPB-COF-H. A Pyrex tube was charged with TAPM (30.4 mg, 0.08 mmol), 1,2,4,5-Tetrakis-(4-formylphenyl) benzene (TPB-H) (39.6 mg, 0.08 mmol), chloroform (2.0 mL), n-butanol (0.1 mL) and 6 M aqueous acetic acid (0.2 mL). After being degassed by freeze-pump-thaw technique for three times and then sealed under vacuum, the tube was placed in an oven at 100 °C for 7 d. The resulting precipitate was filtered, exhaustively washed by Soxhlet extractions with tetrahydrofuran and dichloromethane for 2 d, dried at 120 °C under vacuum for 12 h. The 3D-TPB-COF-H was isolated as white powder (49.7 mg, 77% yield). Elemental analysis for the calculated: C, 88.43%; H, 4.70%; N, 6.87%. Found: C, 84.38%; H, 4.81%; N, 6.63%.

Synthesis of 3D-TPB-COF-Me. A Pyrex tube was charged with TAPM (30.4 mg; 0.08 mmol), 1,2,4,5-Tetrakis-(4-formylphenyl)-3',6'-dimethylbenzene (TPB-Me) (41.8 mg, 0.08 mmol), o-dichlorobenzene (2.0 mL), n-butanol (1.0 mL) and 6 M aqueous acetic acid (0.6 mL). After being degassed by freeze-pump-thaw technique for three times and then sealed under vacuum, the tube was placed in an oven at 110 °C for 7 d. The resulting precipitate was filtered, exhaustively washed by Soxhlet extractions with tetrahydrofuran and dichloromethane for 2 d, dried at 120 °C under vacuum for 12 h. The 3D-TPB-COF-Me was isolated as white powder (48.4 mg, 73% yield). Elemental analysis for the calculated: C, 88.33%; H, 5.02%; N, 6.65%. Found: C, 82.36%; H, 5.06%; N, 6.35%.

Synthesis of 3D-TPB-COF-F. A Pyrex tube was charged with TAPM (30.4 mg; 0.08 mmol), 1,2,4,5-Tetrakis-(4-formylphenyl)-3',6'-difluorobenzene (TPB-F) (42.6 mg, 0.08 mmol), o-dichlorobenzene (0.9 mL), dioxane (2.1 mL) and 12 M aqueous acetic acid (0.3 mL). After being degassed by freeze-pump-thaw technique for three times and then sealed under vacuum, the tube was placed in an oven at 120 °C for 7d. The resulting precipitate was filtered, exhaustively washed by Soxhlet extractions with tetrahydrofuran and dichloromethane for 2 d, dried at 120 °C under vacuum for 12 h. The 3D-TPB-COF-F was isolated as white powder (52.3 mg, 78% yield). Elemental analysis for the calculated: C, 84.69%; H, 4.26%; N, 6.58%. Found: C, 80.12%; H, 4.11%; N, 6.58%.

Acknowledgements

C.W. gratefully acknowledge financial support from the National Natural Science Foundation of China (21772149 and 21572170), the Funds for Creative Research Groups of Hubei Province (2017CFA002) and the Fundamental Research Funds for the Central Universities. J.S. also acknowledge financial support from the National Natural Science Foundation of China (21871009, 21621061 and 21527803), the Swedish Research Council (VR), and the Knut and Alice Wallenberg Foundation (KAW) for financial supports.

Keywords: Three-dimensional • COFs • isostructural • continuous rotation electron diffraction • gas separation

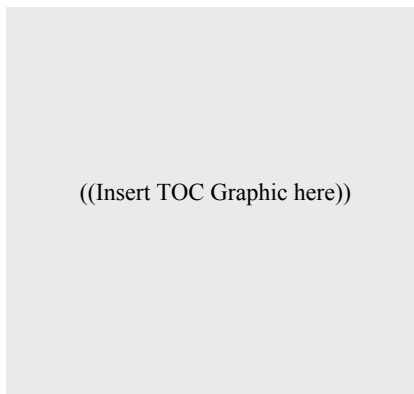
- [1] a) F. Beuerle, B. Gole, *Angew. Chem.* **2018**, *130*, 4942–4972; *Angew. Chem. Int. Ed.* **2018**, *57*, 4850–4878; b) S. Das, P. Heasman, T. Ben, S. Qiu, *Chem. Rev.* **2017**, *117*, 1515–1563; c) C. S. Diercks, O. M. Yaghi, *Science* **2017**, *355*, eaal1585; d) Y. Jin, Y. Hu, W. Zhang, *Nat. Rev. Chem.* **2017**, *1*, 0056; e) N. Huang, P. Wang, D. Jiang, *Nat. Rev. Mater.* **2016**, *1*, 16068; f) J. L. Segura, M. J. Mancheño, F. Zamora, *Chem. Soc. Rev.* **2016**, *45*, 5635–5671; g) S. Y. Ding, W. Wang, *Chem. Soc. Rev.* **2013**, *42*, 548–568.
- [2] a) H. Fan, J. Gu, H. Meng, A. Knebel, J. Caro, *Angew. Chem.* **2018**, *130*, 4147–4151; *Angew. Chem. Int. Ed.* **2018**, *57*, 4083; b) L. Jiang, Y. Tian, T. Sun, Y. Zhu, H. Ren, X. Zou, Y. Ma, K. R. Meihaus, J. R. Long, G. Zhu, *J. Am. Chem. Soc.* **2018**, *140*, 15724; c) Q. Sun, B. Aguilá, L. D. Earl, C. W. Abney, L. Wojtas, P. K. Thallapally, S. Ma, *Adv. Mater.* **2018**, *30*, 1705479; d) Y. Zeng, R. Zou, Y. Zhao, *Adv. Mater.* **2016**, *28*, 2855; e) Z. Kang, Y. Peng, Y. Qian, D. Yuan, M. A. Addicoat, T. Heine, Z. Hu, L. Tee, Z. Guo, D. Zhao, *Chem. Mater.* **2016**, *28*, 1277.
- [3] a) R. Chen, J. L. Shi, Y. Ma, G. Lin, X. Lang, C. Wang, *Angew. Chem.* **2018**, *131*, 6496; *Angew. Chem. Int. Ed.* **2019**, *58*, 6430; b) X. Wang, L. Chen, S. Y. Chong, M. A. Little, Y. Wu, W. H. Zhu, R. Clowes, Y. Yan, M. A. Zwijnenburg, R. S. Sprick, A. I. Cooper, *Nat. Chem.* **2018**, *10*, 1180–1189; c) X. Han, Q. Xia, J. Huang, Y. Liu, C. Tan, Y. Cui, *J. Am. Chem. Soc.* **2017**, *139*, 8693–8697; d) H.-S. Xu, S.-Y. Ding, W.-K. An, H. Wu, W. Wang, *J. Am. Chem. Soc.* **2016**, *138*, 11489–11492; e) V. S. Vyas, F. Haase, L. Stegbauer, G. Savasci, F. Podjaski, C. Ochsenfeld, B. V. Lotsch, *Nat. Commun.* **2015**, *6*, 8508.
- [4] a) P. Wang, F. Zhou, C. Zhang, S.-Y. Yin, L. Teng, L. Chen, X.-X. Hu, H.-W. Liu, X. Yin, X.-B. Zhang, *Chem. Sci.* **2018**, *9*, 8402–8408; b) S. Dalapati, E. Jin, M. Addicoat, T. Heine, D. Jiang, *J. Am. Chem. Soc.* **2016**, *138*, 5797–5800; c) G. Das, B. P. Biswal, S. Kandambeth, V. Venkatesh, G. Kaur, M. Addicoat, T. Heine, S. Verma, R. Banerjee, *Chem. Sci.* **2015**, *6*, 3931–3939.
- [5] a) J. Lv, Y.-X. Tan, J. Xie, R. Yang, M. Yu, S. Sun, M.-D. Li, D. Yuan, Y. Wang, *Angew. Chem.* **2018**, *130*, 12898–12902; *Angew. Chem. Int. Ed.* **2018**, *57*, 12716–12720; b) S. Wang, Q. Wang, P. Shao, Y. Han, X. Gao, L. Ma, S. Yuan, X. Ma, J. Zhou, X. Feng, B. Wang, *J. Am. Chem. Soc.* **2017**, *139*, 4258–4261; c) S. B. Alahakoon, C. M. Thompson, G. Occhialini, R. A. Smaldone, *ChemSusChem* **2017**, *10*, 2116; d) Y. Du, H. Yang, J. M. Whiteley, S. Wan, Y. Jin, S.-H. Lee, W. Zhang, *Angew. Chem.* **2016**, *128*, 1769; *Angew. Chem. Int. Ed.* **2016**, *55*, 1737.
- [6] a) D. D. Medina, T. Sick, T. Bein, *Adv. Energy Mater.* **2017**, *7*, 1700387; b) G. H. Bertrand, V. K. Michaelis, T. C. Ong, R. G. Griffin, M. Dincă, *Proc. Natl. Acad. Sci. U. S. A.* **2013**, *110*, 4923–4928; c) X. Feng, L. Liu, Y. Honsho, A. Saeki, S. Seki, S. Irie, Y. Dong, A. Nagai, D. Jiang, *Angew. Chem.* **2012**, *124*, 2672; *Angew. Chem. Int. Ed.* **2012**, *51*, 2618.
- [7] A. P. Côté, A. I. Benin, N. W. Ockwig, M. O’Keeffe, A. J. Matzger, O. M. Yaghi, *Science* **2005**, *310*, 1166–1170.
- [8] a) A. M. Evans, L. R. Parent, N. C. Flanders, R. P. Bisbey, E. Vitaku, M. S. Kirschner, R. D. Schaller, L. X. Chen, N. C. Gianneschi, W. R. Dichtel, *Science* **2018**, *361*, 52–57; b) B. Gole, V. Stepanenko, S. Rager, M. Grüne, D. D. Medina, T. Bein, F. Würthner, F. Beuerle, *Angew. Chem.* **2018**, *130*, 856–860; *Angew. Chem. Int. Ed.* **2018**, *57*, 846–850; c) K. Wang, L.-M. Yang, X. Wang, L. Guo, G. Cheng, C. Zhang, S. Jin, B. Tan, A. Cooper, *Angew. Chem.* **2017**, *129*, 14337–14341; *Angew. Chem. Int. Ed.* **2017**, *56*, 14149–14153; d) C. Qian, Q. Y. Qi, G. F. Jiang, F. Z. Cui, Y. Tian, X. Zhao, *J. Am. Chem. Soc.* **2017**, *139*, 6736–6743; e) T.-Y. Zhou, S.-Q. Xu, Q. Wen, Z.-F. Pang, X. Zhao, *J. Am. Chem. Soc.* **2014**, *136*, 15885–15888; f) S.-L. Cai, Y.-B. Zhang, A. B. Pun, B. He, J. Yang, F. M. Toma, I. D. Sharp, O. M. Yaghi, J. Fan, S.-R. Zheng, W.-G. Zhang, Y. Liu, *Chem. Sci.* **2014**, *5*, 4693–4700.
- [9] a) H. M. El-Kaderi, J. R. Hunt, J. L. Mendoza-Cortés, A. P. Côté, R. E. Taylor, M. O’Keeffe, O. M. Yaghi, *Science* **2007**, *316*, 268–272; b) D. Beaudoin, T. Maris, J. D. Wuest, *Nat. Chem.* **2013**, *5*, 830–834; c) H. Ma, H. Ren, S. Meng, Z. Yan, H. Zhao, F. Sun, G. Zhu, *Chem. Commun.* **2013**, *49*, 9773–9775; d) Y. B. Zhang, J. Su, H. Furukawa, Y. Yun, F. Gandara, A. Duong, X. Zou, O. M. Yaghi, *J. Am. Chem. Soc.* **2013**, *135*, 16336–16339; e) Q. Fang, S. Gu, J. Zheng, Z. Zhuang, S. Qiu, Y. Yan, *Angew. Chem.* **2014**, *126*, 2922–2926; *Angew. Chem. Int. Ed.* **2014**, *53*, 2878–2882; f) Y. Liu, Y. Ma, Y. Zhao, X. Sun, F. Gándara, H. Furukawa, Z. Liu, H. Zhu, C. Zhu, K. Suenaga, P. Oleynikov, A. S. Alshammari, X. Zhang, O. Terasaki, Omar M. Yaghi, *Science* **2016**, *351*, 365–369.
- [10] a) G. Lin, H. Ding, D. Yuan, B. Wang, C. Wang, *J. Am. Chem. Soc.* **2016**, *138*, 3302–3305; b) G. Lin, H. Ding, R. Chen, Z. Peng, B. Wang, C. Wang, *J. Am. Chem. Soc.* **2017**, *139*, 8705–8709; c) H. Ding, J. Li, G. Xie, G. Lin, R. Chen, Z. Peng, C. Yang, B. Wang, J. Sun, C. Wang, *Nat. Commun.* **2018**, *9*, 5234.
- [11] a) D. N. Bunck, W. R. Dichtel, *Chem. Commun.* **2013**, *49*, 2457–2459; b) L. A. Baldwin, J. W. Crowe, D. A. Pyles, P. L. McGrier, *J. Am. Chem. Soc.* **2016**, *138*, 15134–15137; c) Q. Lu, Y. Ma, H. Li, X. Guan, Y. Yusran, M. Xue, Q. Fang, Y. Yan, S. Qiu, V. Valtchev, *Angew. Chem.* **2018**, *130*, 6150–6156; *Angew. Chem. Int. Ed.* **2018**, *57*, 6042–6048.
- [12] a) T. Ma, E. A. Kapustin, S. X. Yin, L. Liang, Z. Zhou, J. Niu, L.-H. Li, Y. Wang, J. Su, J. Li, X. Wang, W. D. Wang, W. Wang, J. Sun, O. M. Yaghi, *Science* **2018**, *361*, 48–52; b) T. Ma, J. Li, J. Niu, L. Zhang, A. S. Etman, C. Lin, D. Shi, P. Chen, L. H. Li, X. Du, J. Sun, W. Wang, *J. Am. Chem. Soc.* **2018**, *140*, 6763–6766.
- [13] a) X. Han, J. Huang, C. Yuan, Y. Liu, Y. Cui, *J. Am. Chem. Soc.* **2018**, *140*, 892–895; b) O. Yahiaoui, A. N. Fitch, F. Hoffmann, M. Froba, A. Thomas, J. Roeser, *J. Am. Chem. Soc.* **2018**, *140*, 5330–5333.
- [14] O. Sitsel, S. Raunser, *Nat. Chem.* **2019**, *11*, 106–108.
- [15] a) H. Chen, J. Ju, Q. Meng, J. Su, C. Lin, Z. Zhou, G. Li, W. Wang, W. Gao, C. Zeng, C. Tang, J. Lin, T. Yang, J. Sun, *J. Am. Chem. Soc.* **2015**, *137*, 7047–7050; b) W. Hua, H. Chen, Z.-B. Yu, X. Zou, J. Lin, J. Sun, *Angew. Chem.* **2014**, *126*, 5978–5981; *Angew. Chem. Int. Ed.* **2014**, *53*, 5868–5871; c) Y. Wang, T. Yang, H. Xu, X. Zou, W. Wan, *J. Appl. Cryst.* **2018**, *51*, 1094–1101; d) Y. Wang, S. Takki, O. Cheung, H. Xu, W. Wan, L. Ohrstrom, A. K. Inge, *Chem. Commun.* **2017**, *53*, 7018–7021; e) J. Li, J. Sun, *Acc. Chem. Res.* **2017**, *50*, 2737–2745.
- [16] a) E. Gagnon, T. Maris, P.-M. Arseneault, K. E. Maly, J. D. Wuest, *Cryst. Growth Des.* **2010**, *10*, 648–657; b) P. Ganesan, X. Yang, J. Loos, T. J. Savenije, R. D. Abellon, H. Zuilhof, E. J. R. Sudholter, *J. Am. Chem. Soc.* **2005**, *127*, 14530–14531.
- [17] a) W. Kabsch, *Acta Cryst.* **2010**, *D66*, 133–144; b) W. Wan, J. Sun, J. Su, S. Hovmoller, X. Zou, *J. Appl. Cryst.* **2013**, *46*, 1863–1873; c) G. M. Sheldrick, *Acta Cryst.* **2015**, *A71*, 3–8; d) L. Palatinus, G. Chapuis, *J. Appl. Cryst.* **2007**, *40*, 786–790; e) A. L. Spek, *Acta Cryst.* **2009**, *D65*, 148–155.
- [18] L. Du, Z. Lu, K. Zheng, J. Wang, X. Zheng, Y. Pan, X. You, J. Bai, *J. Am. Chem. Soc.* **2013**, *135*, 562–565.

Entry for the Table of Contents (Please choose one layout)

Layout 1:

RESEARCH ARTICLE

Text for Table of Contents



Author(s), Corresponding Author(s)*

Page No. – Page No.

Title

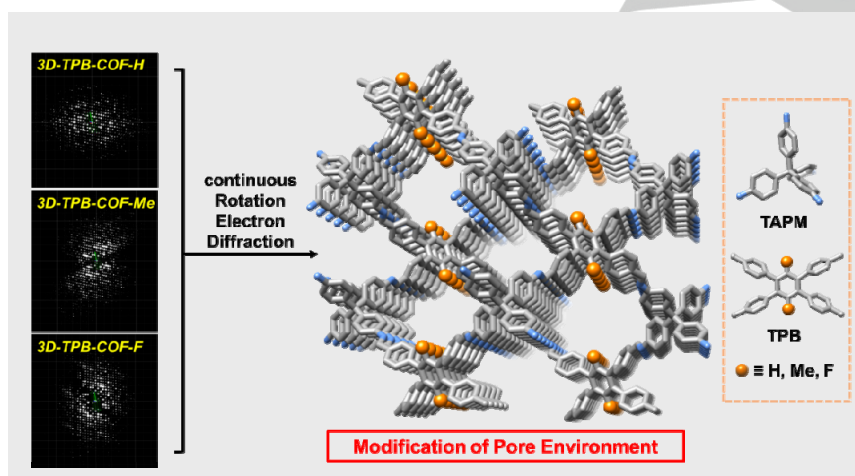
Layout 2:

RESEARCH ARTICLE

Chao Gao, Jian Li, Sheng Yin, Guiqing Lin, Tianqiong Ma, Yi Meng, Junliang Sun* and Cheng Wang*

Page No. – Page No.

Isostructural 3D Covalent Organic Frameworks



Isostructural 3D Covalent Organic Frameworks: Three isostructural 3D COFs functionalized with organic groups –H, –Me and –F, which have similar crystallinity and topology, have been reported. The resolution of the continuous rotation electron diffraction (cRED) datasets reached up to 0.9-1.0 angstrom, leading to the location of all non-hydrogen atomic positions directly by 3D ED techniques for the first time.